The Astrophysical Journal, 1000:116 (11pp), 2026 March 20 https://doi.org/10.3847/1538-4357/ae473b

Globular Clusters GMRT Pulsar Search (GCGPS). II. Discovery of Five Millisecond Pulsars in M69 and M70

Jyotirmoy Das[1], Jayanta Roy[1], Paulo C. C. Freire[2], Scott Ransom[3], Bhaswati Bhattacharyya[1], Karel Adamek[4], Wes Armour[5], Sanjay Kudale[1,6], and Mekhala V. Muley[6]
[1] National Centre for Radio Astrophysics (NCRA), Pune-411007, Maharashtra, India
[2] Max-Planck-Institut für Radioastronomie (MPIfR), Auf dem Hügel 69-53121, Bonn, Germany
[3] National Radio Astronomy Observatory (NRAO), Charlottesville, VA, USA
[4] Department of Physics, Silesian University in Opava, Opava, 74601, Czechia
[5] Oxford e-Research Centre (OeRC), University of Oxford, Oxford, OX1 3PJ, UK
[6] Giant Metrewave Radio Telescope (GMRT), Khodad, Pune-410504, Maharashtra, India
Received 2025 December 11; revised 2026 February 13; accepted 2026 February 16; published 2026 March 17

Abstract

This paper reports recent discoveries from the Globular Clusters GMRT Pulsar Search survey, which aims to uncover pulsars in the globular clusters (GCs) of the Milky Way using the upgraded Giant Metrewave Radio Telescope (uGMRT). Utilising the Band-4 (550–750 MHz) and Band-3 (300–500 MHz) receivers, the survey targets GCs accessible to uGMRT ($-53^\circ < \delta < -17^\circ$), excluding the declination range that can be covered by the Five-hundred-meter Aperture Spherical radio Telescope. The survey focuses on GCs that have not previously been searched with comparable sensitivity in these radio frequencies. In this paper, we present the discovery of five millisecond pulsars (MSPs) in two GCs, NGC 6637 (Messier69/M69) and NGC 6681 (Messier70/M70), each hosting MSPs identified here for the first time. Observations of M69 led to the discovery of two MSPs: J1831−3220A (M69A) and J1831−3220B (M69B), one of which (M69A) we localize with arcsecond precision using interferometric imaging and targeted follow-up, and the other (M69B) remains unlocalised due to sensitivity constraints. Observations of M70 resulted in three new MSPs: J1843−3217A (M70A), J1843−3217B (M70B), and J1843−3217C (M70C). Although direct imaging did not yield precise localizations for these MSPs, we provide initial estimates based on uGMRT beam forming and imaging analysis. Additionally, we present preliminary imaging results for other observed GCs, and in cases of nondetections, we report upper limits on pulsed emission based on the rms noise levels in the image plane.

Unified Astronomy Thesaurus concepts: Millisecond pulsars (1062); Globular star clusters (656); Radio astronomy (1338); Neutron stars (1108); Binary pulsars (153)

1. Introduction

The close interaction between an old neutron star (NS) and a low-mass star can lead to the formation of a low-mass X-ray binary (LMXB) system (V. Kalogera & R. F. Webbink 1996, 1998; V. Kalogera 1998). In such systems, the NS accretes matter from its companion, gradually spinning up in the process. The high stellar densities and interaction rates found in globular clusters (GCs; F. Verbunt & P. Hut 1987; D. Pooley et al. 2003; A. Bahramian et al. 2013) make them ideal environments for the dynamical formation of LMXBs—an occurrence that is rare in the Galactic disk. As a result, GCs host approximately 10^3 more LMXBs per unit mass than the Galactic disk (C. L. Sarazin et al. 2003). Over time, these LMXBs evolve into pulsars with spin periods of just a few milliseconds, known as recycled or millisecond pulsars (MSPs); generally with spin periods $P_s < 20$ ms (W. Becker & J. Trümper 1999) and low magnetic fields ($B \sim 10^8$–10^{10} G), usually accompanied by a low-mass white dwarf ($M_{WD} < 0.20\,M_\odot$; see A. G. Istrate et al. 2014) or a nondegenerate companion (for a review, see T. M. Tauris & E. P. J. van den Heuvel 2023). The abundance of LMXBs in GCs leads to a correspondingly high population of MSPs: of the >700 known MSPs, ∼340 are located in GCs.[7]

The high stellar densities of GCs mean that some MSP binaries have properties unlike any found in the Galactic disk, such as high orbital eccentricities and massive companions. These binaries result from exchange encounters that happen after the pulsar is recycled. These unusual characteristics make them, potentially, powerful probes for studying gravity in the strong-field regime. For instance, J0514−4002E in NGC 1851 might be an MSP–black hole system (E. D. Barr et al. 2024), which could allow tests of alternative gravity theories beyond the current capabilities of binary pulsar timing (P. C. C. Freire & N. Wex 2024).

These rare systems highlight the importance of continued pulsar searches in GCs. This is one of the main motivations of the Globular Clusters GMRT Pulsar Search (GCGPS) survey. This survey, including a more complete motivation, target selection, and technical details, is discussed in detail by J. Das et al. (2025), which is Paper I in this series; it is also the designation we will use throughout this work.

In this work (Paper II), we provide an update on the current status of the survey and its data analysis in Section 2. In Section 3, we report the discovery of five MSPs in NGC 6637

[7] Based on data from the ATNF pulsar catalog, https://www.atnf.csiro.au/research/pulsar/psrcat/ (R. N. Manchester et al. 2005) and Paulo Freire's GC pulsar list, see https://www3.mpifr-bonn.mpg.de/staff/pfreire/GCpsr.html; the total number of known pulsars in GCs is currently 359.

(M69) and NGC 6681 (M70). In Section 4, we present the radio imaging analysis of the GCGPS-observed clusters, which helps localize the newly discovered pulsars, and provides a set of unassociated faint radio sources, worth following up for potential new MSPs, along with flux-density upper limits for the nondetections. The final imaging data (in FITS format) associated with this paper are also made publicly available (doi:10.5281/zenodo.17781807), offering a valuable resource for planning more targeted and sensitive follow-up searches. Finally, we summarize our findings in Section 5.

2. Observations and Survey Status

The GCGPS observations began in 2023 May. In each half-yearly uGMRT cycle, we observe a subset of the selected GCs to search for new MSPs. Each GC is observed using two simultaneously formed phased array (PA) beams, one formed with the central square (CSQ) antennas and the other using antennas up to the third arm, in either Band-3 or Band-4, depending on the target. This configuration ensures the best sensitivity possible with the uGMRT across both the full cluster and its core. For GCs with known MSPs, we record coherently dedispersed (CD) PA data at median GC dispersion measure (DM) with a time resolution of 40.96 μs and 512 frequency channels across a 200 MHz bandwidth. For GCs with no known MSPs a priori, we record standard PA data with 81.92 μs time resolution and 4096 channels, without any coherent dedispersion. Alongside beam data, we also record the interformatric data to image the GC field for further analysis. The data analysis procedures followed here are the same as those described in detail in Paper I.

Of the 31 GCs initially targeted in Phase-I (listed in Table 2 of Paper I), we have to date completed observations and data analysis for one GC in Band-3 and 21 GCs in Band-4 (see Table 1). Although NGC 5897 was listed as a Band-3 target in Table 2 of Paper I, it was observed in Band-4 instead due to feed-rotation constraints, and its Band-4 analysis is therefore presented in this paper. Based on this progress, approximately 50% of the planned Phase-I survey is complete in Band-3, and about 73% is complete in Band-4. So far, this survey has led to the discovery of seven MSPs in four GCs where no pulsars were previously known.[8] The first discovery of this survey, J1617−2258A in NGC 6093, along with the survey details and its timing follow-up, was presented in Paper I. In this paper, we report five additional discoveries in NGC 6637 (Messier69/M69) and NGC 6681 (Messier70/M70), present their initial study and imaging analysis of all observed and analyzed GCs.

Apart from the GCs observed and analyzed so far in this survey (a subset of the Phase-I targets), Table 1 lists their observational details. The remaining Phase-I observations, as well as the planned Phase-II observations—which will include several GCs previously excluded in Phase-I due to sensitivity limits or restricted sky coverage—are currently ongoing. These Phase-II observations are being carried out using the newly commissioned multibeam SPOTLIGHT[9] (J. Roy et al. 2024) backend, which provides significantly higher sensitivity along with multibeam coverage (currently ∼160 post correlation/PC beams), substantially exceeding the single-pointing capability of the Phase-I GCGPS survey. The MeerKAT's TRAPUM (F. Abbate et al. 2022; A. Ridolfi et al. 2022) survey, currently the most prominent survey in the southern hemisphere,[10] has greatly benefited from the large number of beams provided by a similar beamformer installed at the MeerKAT telescope, the Filterbanking Beamformer User Supplied Equipment (FBFUSE, E. D. Barr 2018; W. Chen et al. 2021). This has been especially useful for surveys of extended GCs (J. Chen et al. 2023).

A full-array 30 antenna phased uGMRT Band-4 PC beam is expected to provide a theoretical sensitivity roughly ∼2 times higher than the scaled L-band sensitivity of TRAPUM (see Section 3.3 of Paper I for details). This improvement in both sensitivity and sky coverage will allow us to observe targets that were earlier excluded because of limited coverage or comparatively lower sensitivity. The results from these ongoing and upcoming observations will be presented in future publications from this survey.

3. Discoveries

We now report the discovery of five MSPs in the PA beam data of two GCs with no previously known pulsars and provide a detailed summary of their initial parameters.

3.1. Discoveries in NGC 6637 (M69)

As shown in Table 1, we observed M69 in 2024 May for 2 hours of on-source time as part of the GCGPS survey. As described in Section 2, two simultaneous uGMRT Band-4 PA beams: the CSQ beam and the third-arm beam, were formed to observe M69 with optimal sensitivity for pulsar discovery. We adopted the predicted DM of the YMW16 model ($DM^{*} = 119.8\,pc\,cm^{-3}$; see J. M. Yao et al. 2017) and searched a DM range of 40–180 pc cm^{-3} (following the DM search strategy detailed in Paper I) with a DM step of 0.1 pc cm^{-3}. An initial PRESTO[11] (S. Ransom 2011)-based acceleration search with a maximum 200 bin-drift correction ($Z_{max} = \pm 200$) was performed on the CSQ data using our CPU-based pipeline Pulsar Search Script (PSS)[12] .This search led to the discovery of J1831–3220A, hereafter referred to as M69A. With a spin period of $P_s \sim 3.81$ m*s*, this pulsar was detected at a DM of 82.1 pc cm^{-3}; a subsequent finer search refined this value to $DM_{M69A} = 82.12\,pc\,cm^{-3}$. The discovery signal-to-noise ratio (SNR) from the PRESTO PREPFOLD folding of the CSQ data was 17.5σ.

Following this detection, we performed a more sensitive search to identify lower-SNR candidates, covering the DM range $DM_{M69A} \pm 15\,pc\,cm^{-3}$ with a finer DM step of 0.02 pc cm^{-3}. This search resulted in the detection of a second candidate, which was later confirmed in a follow-up observation as J1831–3220B, hereafter M69B. The discovery SNR of this pulsar in the CSQ data was approximately 10σ, with a spin period of $P_s \sim 4.80$ ms and a measured DM of 81.92 pc cm^{-3}.

Having third-arm-beam central theoretical sensitivity ∼1.57 ($N_2/N_1 = 22/14$) times that of the CSQ-beam central sensitivity, a general acceleration search over the DM space $DM_{M69A} \pm 15\,pc\,cm^{-3}$ with a DM step 0.02 pc.cm^{-3} was also performed on the third-arm data for pulsars situated close to the GC center, but no promising candidates were detected.

[8] See the survey webpage: http://www.ncra.tifr.res.in/~jroy/GC.html.
[9] The SPOTLIGHT website: https://spotlight.ncra.tifr.res.in/.
[10] The survey website: https://www.trapum.org/.
[11] GitHub link of PRESTO repository: https://github.com/scottransom/presto.
[12] Available at https://github.com/jyotirmoydas5392/Pulsar_Search_Script.

Table 1
The List of GCs Observed and Analysed So Far under the GCGPS Survey

GC Name (NGC XXXX)	Obs. Epoch MJD	uGMRT BAND (BAND-4/3)	Obs. Mode (PA/CD)	On-source Time (s)	Beam Center (R.A., Decl.) (hh:mm:ss, dd:mm:ss)	S^{c}_{min} (μJy)	S^{p}_{min} (μJy)
NGC 1904	60282	BAND-4	PA	9060	(05 24 11.09, −24 31 29.0)	112	71
NGC 4590	60273	BAND-4	PA	8220	(12 39 27.98, −26 44 38.6)	413	270
NGC 5286	60608	BAND-4	PA	6960	(13 46 26.81, −51 22 27.3)	361	236
NGC 5897	60447	BAND-4	PA	6960	(15 17 24.50, −21 00 37.0)	201	131
NGC 5986	60110	BAND-4	CD	4560	(15 46 03.00, −37 47 11.1)	173	117
NGC 6093	60126	BAND-4	PA	8220	(16 17 02.41, −22 58 33.9)	132	86
NGC 6139	60372	BAND-4	PA	7560	(16 27 40.37, −38 50 55.5)	1553	869
NGC 6293	60664	BAND-4	PA	7200	(17 10 10.20, −26 34 55.5)	802	544
NGC 6333	60447	BAND-4	PA	7440	(17 19 11.26, −18 30 57.4)	186	117
NGC 6355	60632	BAND-4	PA	8580	(17 23 58.59, −26 21 12.3)	532	348
NGC 6388	60066	BAND-4	PA	5400	(17 36 17.23, −44 44 07.8)	146	92
NGC 6528	60664	BAND-4	PA	7260	(18 04 49.64, −30 03 22.6)	353	231
NGC 6541	60357	BAND-4	PA	9660	(18 08 02.36, −43 42 53.6)	261	171
NGC 6553	60632	BAND-4	PA	7560	(18 09 17.60, −25 54 31.3)	98	62
NGC 6569	60981	BAND-4	PA	7860	(18 13 38.80, −31 49 36.8)	120	78
NGC 6637	60447	BAND-4	PA	6960	(18 31 23.10, −32 20 53.1)	92	62
NGC 6638	60981	BAND-4	PA	9660	(18 30 56.10, −25 29 50.9)	72	45
NGC 6642	60379	BAND-4	PA	9000	(18 31 54.10, −23 28 30.7)	125	85
NGC 6652	60632	BAND-4	CD	7080	(18 35 45.63, −32 59 26.6)	241	163
NGC 6681	60431	BAND-4	PA	8640	(18 43 12.76, −32 17 31.6)	212	112
NGC 6723	60146	BAND-4	PA	8160	(18 59 33.15, −36 37 56.1)	456	277
NGC 6809	60421	BAND-3	PA	13560	(19 39 59.71, −30 57 53.1)	511	322

Note. The "Obs. epoch" is the Modified Julian Date (MJD) at which the associated GC was observed. The uGMRT bands used under the GCGPS survey are Band-3 (330–500 MHz) and Band-4 (550–650 MHz), and the associated band for each GC observation is mentioned in the column titled "uGMRT BAND." The PA and CD in the "Obs. mode" stand for the "phased array" and "coherently dedispersed" mode, whichever was used to take the data, as discussed in Section 2. For all the observations, the beam was formed at the GC center and the GC center R.A (J2000) and decl. (J2000) values were taken from the W. E. Harris list of GC parameters (W. E. Harris 1996, 2010 edition). S^{c}_{min} is the continuum 10σ, and S^{p}_{min} is the PA/CD beam data 10σ detection limit for each observation (see Section 4.3).

To obtain the initial positional estimates, we folded the third-arm data for these two MSPs. The detection significance in both cases was reduced by a factor of 40%–60% compared to the CSQ detection, suggesting that the MSPs are located away from the cluster center, where the CSQ beam has 40%–60% higher sensitivity than the third-arm beam. Based on this estimate, we performed imaging of the field to localize the MSPs; this is discussed in Section 4.1.

During the discovery observation, M69A was detected with a significant acceleration ($P_{dot} \sim 10^{-12}$), confirming that it is a binary MSP in a relatively compact orbit. For M69B, we could not detect any significant acceleration, indicating that it is an isolated or an MSP in a binary orbit wide enough so that 2 hr of on-source time is not enough to detect the orbital acceleration. Timing follow-up observations are underway to obtain precise timing solutions for these systems, which we plan to publish in a subsequent paper as part of this survey.

3.2. Discoveries in NGC 6681 (M70)

Similar to the M69 observation, M70 was observed in 2024 May as part of the GCGPS survey (observation details in Table 1). Two simultaneous uGMRT Band-4 PA beams, the CSQ beam and the third-arm beam, were formed to observe M70 with optimal sensitivity for pulsar discovery. Using the YMW16 model predicted DM ($DM^{*} = 105.2\,pc\,cm^{-3}$), and following the same search strategy as for M69, we performed an acceleration search with $Z_{max} = \pm 200$, over a DM range of 30–160 pc cm^{-3} with a DM step of 0.1 pc cm^{-3}. The search on the CSQ data led to the discovery of three MSPs in this GC. PSR J1843–3217A, hereafter M70A, an MSP with a spin period of $P_s \sim 3.93$ ms, was detected at a DM of $\sim$70.9 pc cm^{-3} with an SNR of $\sim 23.67\sigma$. The strongest detection was from J1843–3217B (M70B; $P_s \sim 4.44$ ms), identified at a DM of 71.2 pc cm^{-3} with an SNR of about 34.55σ. The faintest of the three, J1843–3217C (M70C; $P_s \sim 6.06$ ms), was detected at a

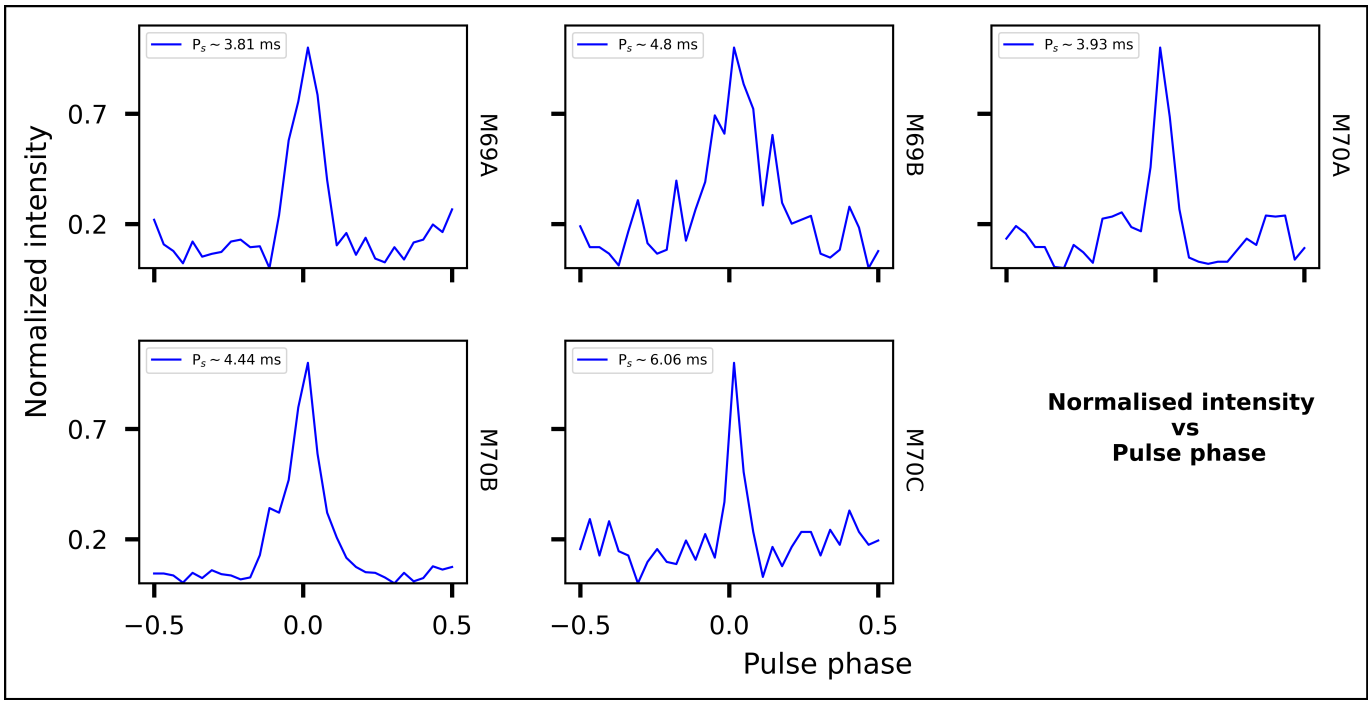

Figure 1. The normalized pulse profiles at uGMRT Band-4 (550–750 MHz) for the five MSPs discovered in two globular clusters as part of the GCGPS survey are shown. The first two profiles (left to right) are the M69A and M69B from NGC 6637 (Messier69/M69), and the remaining (in the same order) are the M70A, M70B, and M70C from NGC 6681 (Messier70/M70).

Table 2
This Table Presents the Details of Five MSPs Discovered as Part of the GCGPS Survey

GC Name (NGC XXXX)	Pulsar	Period (ms)	DM (pc cm^{-3})	Discovery SNR (CSQ (σ), Third Arm (σ))	R.A. (J2000) and Decl. (J2000) (hh:mm:ss, dd:mm:ss)	S_ν (650 MHz) (μJy)
NGC 6637	M69A	3.81	82.12	(17.5, 11.2)	(18:31:22.43, −32.20.47.36)	224 ± 13
(Messier69/M69)	M69B	4.80	81.92	(10.0, 7.6)	TBC	TBC
NGC 6681	M70A	3.93	70.65	(34.3, 47.8)	TBC	TBC
	M70B	4.44	71.14	(16.9, 23.7)	TBC	TBC
(Messier70/M70)	M70C	6.06	71.06	(11.6, 16.8)	TBC	TBC

Note. Two of these MSPs are located in NGC 6637 (Messier69/M69), while the remaining three are in NGC 6681 (Messier70/M70). For each pulsar, key discovery parameters—including spin period, dispersion measure (DM), PRESTO PREPFOLD signal-to-noise ratio (SNR), and initial localized position (where confirmed)—are provided based on the discovery observations, initial imaging, and beam simulation analysis. For the localized MSP (M69A)in the image plane, we also provide the measured flux density (S_ν, at 650 MHz) from the image analysis. The unconfirmed results are marked with "TBC" to be confirmed), wherever applicable in the table.

DM of ∼71.1 pc cm^{-3} with an SNR of 12.06σ in the CSQ data. Following these detections, more precise DM values for each MSP were determined using targeted PRESTO-based searches around the initial detection DMs; the refined values are listed in Table 2.

All these MSPs were redetected in the simultaneously recorded third-arm data with increased SNR. For all of them, the increment in SNR is about 40%–60%, confirming the MSP discovery. This also suggests that they are situated very close to the GC center, and inside the half-power beamwidth of the third-arm PA beam. A detailed discussion on the localization is done in Section 4.1. Similar to M69, we also performed an acceleration search on the third-arm data over DM* ± 15 pc cm^{-3} with DM step =0.02 pc cm^{-3}, to detect the MSPs that are very close to the GC center, and might have been missed in the less sensitive CSQ search, but we could not detect any promising candidates.

Including the two MSPs in M69, the normalized pulse profiles of all five MSPs are shown in Figure 1, with their corresponding parameters listed in Table 2. In addition, the PRESTO PREPFOLD outputs for all five MSPs are provided in Appendix A.

4. Imaging of the GCGPS-observed GCs

From the simultaneously recorded interferometric data, we imaged all GCGPS-observed GCs using the automated pipeline CAPTURE. The CAPTURE pipeline is designed to process uGMRT interferometric data in an automated manner, provided the observations follow a standard imaging strategy. Originally, the pipeline required the presence of a dedicated standard flux calibrator to perform absolute flux calibration. However, for several GCGPS observations, we prioritized longer on-source integration time and therefore did not observe a standard flux calibrator. Instead, only bright phase calibrators

were observed as part of the phasing operations. To enable imaging of these nonstandard datasets, we modified the pipeline to perform flux calibration using the observed phase calibrators by manually supplying appropriate calibrator models. These models were constructed using the most recent multiband observations (from GCGPS survey as well) or measurements (mostly from Very Large Array (VLA) calibrator database)[13] available for the corresponding phase calibrators. The adopted flux densities and spectral indices were further validated using existing GCGPS observations that included standard 3C flux calibrators, with the same phase calibrator used as a common reference. This confirmed that the flux densities derived for the phase calibrators are consistent with their cataloged values. This approach eliminated the need for dedicated flux calibrator observations and enabled reliable imaging of the observed GC fields while maximizing on-source integration time.

4.1. Localization of Pulsars

As discussed in Sections 3.1 and 3.2, both GCs were observed simultaneously using the CSQ and third-arm PA beams during the discovery observations. Aided by beam multibeam (CSQ and the third arm) detection, the imaging from the interferometric data allowed us to localize the MSPs within the image field efficiently, provided they were detectable as point sources.

Imaging of M69 revealed multiple radio sources within the field, some of which could correspond to the newly discovered MSPs. To identify the most likely candidates, we used the detection SNR between the CSQ and third-arm beams from the discovery observation, along with beam simulation and radiometer equation (R. J. Dewey et al. 1985) estimated fluxes. The third-arm-to-CSQ SNR ratios for PSRs M69A and M69B were approximately 0.64 and 0.76, respectively. We simulated the beam responses for both the CSQ and third-arm beams during the discovery observation using the uGMRT beam simulation tool `uGMRT_beam_fov.py`. Based on the observed SNR ratios and the beam response model, we estimated the radial offsets of the MSPs to be within $\sim$15″–30″ from the cluster center. Guided by these estimates, along with estimated fluxes, imaging revealed two promising point source candidates consistent with the expected positions of the MSPs, along with two additional point sources located slightly farther from the predicted radial range. In subsequent timing follow-up observations, each of the four candidate positions was targeted with two simultaneous beams centered on their respective locations. The resulting third-arm-to-CSQ SNR ratios confirmed that one of the two inner candidates corresponds to the newly discovered M69A, while we couldn't associate M69B with any of the remaining three compact radio sources, constrained by the poor detection significance. The localized position of the M69A and the associated point source is shown in Figure 2, and the R.A., decl., and measured flux density from the image is listed in Table 2. The inner one (maked as "A") and the outer two candidates (marked as "B" and "C" in Figure 2), which we couldn't associate with other discovered MSP M69B, or any other known pulsars, remain strong candidates for potential MSPs or even M69B as well.

[13] The VLA calibrator database: https://science.nrao.edu/facilities/vla/observing/callist.

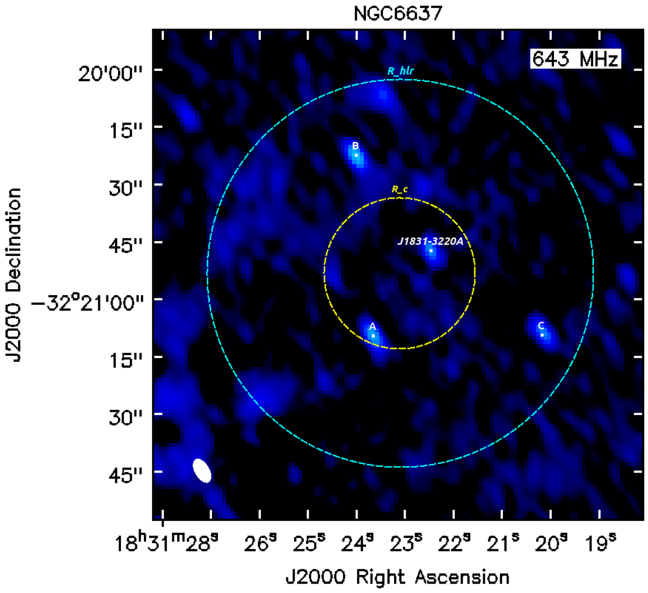

Figure 2. The uGMRT Band-4 radio image of the GC field M69, generated using the automated pipeline `CAPTURE`. The image shows the localized position of J1831–3220A (M69A), along with the marked core and half-light radius of the cluster. Any of the three sources ("A", "B", and "C") could be associated with J1831–3220B (M69B), or probably be some new MSPs as well.

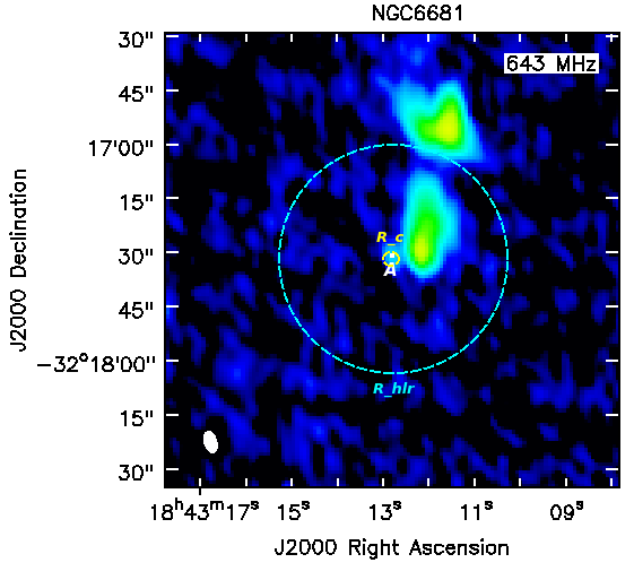

Figure 3. The `CAPTURE` generated uGMRT Band-4 radio image of the GC field M70, where we can see the bright extended source close to the GC center, which prevented us from localizing the MSPs in the image plane.

For the three MSPs in M70 (M70A, M70B, and M70C), the third-arm-to-CSQ-detection SNR ratios were approximately 1.39, 1.49, and 1.45, respectively. Similar to our analysis for M69, we simulated the uGMRT beam responses (CSQ and third arm) at the time of the discovery observation for M70 and used the observed SNR ratios to estimate the likely radial positions of the MSPs within the field. The simulations suggest that the expected positions of all three MSPs lie within $\sim$10″ of the cluster center, with the highest probability density concentrated at the very core. Imaging of M70 revealed a relatively strong, extended radio source located near the cluster

center, which is unlikely to be associated with any of the MSPs due to its morphology and high flux density. In addition to this, a fainter, compact point source was detected almost exactly at the cluster center, marked as "A" in Figure 3. Given its compactness and alignment with the predicted positions, this source is a promising candidate for any of the three MSPs. No other plausible sources were identified within the cluster region. However, dedicated timing follow-up is required to confirm their actual positions and to establish a definitive association with the imaged source.

4.2. The GC Images

We present all 22 beam-processed GC images in the Appendices, grouped into three sets (see Appendix B, Figures 5, 6, and 7). These images reveal a wealth of information about each GC field, providing a valuable basis for extracting further scientific insights.

The clusters NGC 5986 and NGC 6652 had known MSPs prior to the GCGPS observations. In the case of NGC 5986, the imaging revealed several faint compact sources (with flux densities of a few hundred μJy) located outside the half-light radius, which could be potential MSP candidates. However, the lack of a well-localized position for the previously discovered pulsar in this cluster (J1546–3747A) did not allow us to associate it with any of the detected sources in the image field. For NGC 6652, similar to the findings of T. Gautam et al. (2022), we detect the source that they associated with J1835–3259B (marked in the image), but no findings for J1835–3259A, along with several other faint compact sources that are not associated with any known radio emitters. These additional detections are promising candidates for follow-up studies aimed at identifying new MSPs.

There are now four GCs (NGC 1904, NGC 6093, NGC 6637, and NGC 6681) that host the first known MSPs for each GC, discovered through the GCGPS survey. For NGC 1904, the localization work for the GCGPS-discovered pulsar NGC 1904A (J0524–2431A) is currently ongoing. We include the image of NGC 1904 in this paper for completeness. In NGC 6093, three MSPs are currently known: the first discovered by the GCGPS survey (Paper I), and two subsequently found by the TRAPUM survey.[14] Of these, only NGC 6093A (J1617–2258A) has a well-localized position (from Paper I), which we mark in the image. Similarly, for NGC 6637, the localized MSP (M69A) discovered in this work is marked in its image. The image of NGC 6681 is also presented, although the positions of the MSPs discovered by TRAPUM in this cluster (three more after the first three discoveries from the GCGPS survey) are not yet publicly available. Across all four clusters, the images reveal several faint yet compact, unassociated radio sources. These may correspond to the GCGPS-discovered unlocalised MSPs (for NGC 1904, NGC6637, and NGC 6681), or TRAPUM-discovered MSPs (in NGC 6093 and NGC 6681), whose positions are not yet released, or they could represent entirely newundiscovered MSPs. These sources warrant targeted follow-up observations.

Except for these 6 GCs, 16 additional clusters in the GCGPS survey resulted in nondetections and currently do not host any known MSPs. For most of these clusters, the imaging reveals several previously unassociated compact radio sources, which could plausibly include yet-undiscovered MSPs. To enable dedicated follow-up observations of these clusters with deeper sensitivity, we publish the processed CASA FITS images along with this paper (see doi:10.5281/zenodo.17781807). We appreciate using these images to identify and prioritize promising targets for future searches.

4.3. Nondetection Limits

To estimate the nondetection limit of the undiscovered GC MSPs from the GCGPS observations, we utilize imaging data along with the correlation between continuum emission and the pulsar radiometer equation. This approach allows for a more accurate estimation of detection limits—via the derived $S_{\rm min}$ from the GC images—as it inherently accounts for sensitivity losses caused by scintillation or the presence of radio frequency interference (RFI), both of which can lead to suboptimal phasing.

According to R. J. Dewey et al. (1985), for continuum emission, the radiometer equation can be written as

$$S_{\rm min} = \frac{\mathrm{SNR} * T_{\rm sys} * \beta}{G\sqrt{N(N-1)n_{\rm pol}\mathrm{BW}\Delta t_{\rm obs}}}, \quad (1)$$

whereas, for time-domain PA beamforming observation, we can write

$$S_{\rm min} = \frac{\mathrm{SNR} * T_{\rm sys} * \beta}{G \times N\sqrt{n_{\rm pol}\mathrm{BW}\Delta t_{\rm obs}}} \times \sqrt{\frac{W_{\rm eff}}{P_{\rm s} - W_{\rm eff}}}. \quad (2)$$

Using Equations (1) and (2), we can write

$$S^{p}_{\rm min} = S^{c}_{\rm min} \times \frac{\sqrt{N_1(N_1-1)}}{N_2} \times \sqrt{\frac{W_{\rm eff}}{P_{\rm s} - W_{\rm eff}}}, \quad (3)$$

where all the parameters carry their standard meaning. Here, N_1 is the number of antennas used for the continuum observation, and N_2 is the number of antennas used for the PA/CD beamforming observation. In GCGPS, for continuum recording, we always used all the available antennas at the time of the observation, which typically ranged from 27 to 30. For beamforming observation, for the central square (CSQ) PA/CD beam, the expected number of antennas is 14 (all the central square antennas), and for the third-arm beam, it is 22 (taking up to the third antenna in each arm for beam formation).

Using Equation (3) and the rms value derived from the imaging data ($S^{c}_{\rm min}$), we calculate the beam central sensitivity ($S^{p}_{\rm min}$) achieved in our beamformed observations. For each GC, we take into account the number of antennas used for the continuum observations (N_1) as well as for the beamforming observations (N_2) while calculating the nondetection limits. For the beamforming nondetection limits, we assume a duty cycle ($\frac{W_{\rm eff}}{P_{\rm s}}$) of 0.1 (10%), which is a reasonable assumption for the typical MSP population. In Table 1, for each GC, we present the 10σ nondetection limits for both the continuum and the CSQ PA/CD beam at the observed band. Similarly, for the third-arm PA/CD beam, we can calculate the achieved beam central sensitivity (nondetection limit) using Equation (3). For the third-arm PA/CD beam, this sensitivity ($S^{p}_{\rm 3rdarm\_min}$) will scale by a factor of $\sim$1.57 compared to $S^{p}_{\rm CSQ\_min}$, following the

[14] See https://www3.mpifr-bonn.mpg.de/staff/pfreire/GCpsr.html.

relation $S^{p}_{3\mathrm{rdarm\_min}} = S^{p}_{\mathrm{CSQ\_min}} \times \left(\frac{N_2^{\mathrm{CSQ}}}{N_2^{3\mathrm{rdarm}}}\right)$, where theoretically $N_2^{\mathrm{CSQ}} = 14$ and $N_2^{3\mathrm{rdarm}} = 22$.

5. Summary

This paper presents the discovery of five MSPs from GCGPS. All these MSPs are the first MSPs to be discovered in the respective GCs.

The GCGPS observation of the GC NGC 6637 (M69) resulted in the discovery of two MSPs: M69A is a 3.80 ms MSP (DM = 82.12 pc cm^{-3}), it was detected with a significant acceleration ($\dot{P} \sim 10^{-12}$) during the discovery observation, confirming it's a binary in a relatively compact orbit; whereas M69B, a 4.80 ms MSP (DM = 81.92 pc cm^{-3}), was detected with no acceleration, suggesting it is isolated or a binary system in a wide orbit. We localize M69A in the image plane (see Figure 2 and Table 2) with arcsec precision, by simulating the discovery uGMRT beams along with using the simultaneously recorded image data during discovery observation and subsequent follow-up observations.

The observation of NGC 6681 (M70) led to the discovery of three new MSPs. M70A is a 3.93 ms pulsar with a DM of 70.65 pc cm^{-3}. The brightest among them is M70B, a 4.44 ms MSP with a DM of 71.14 pc cm^{-3}, while the faintest is M70C, a 6.06 ms MSP with a DM of 71.06 pc cm^{-3}. None of these sources exhibited detectable acceleration over the 2.5 hr discovery observation, indicating they are either isolated or in binary systems with relatively wide orbits. As in the case of M69, the beam simulation, along with the detection ratios of both beams (CSQ and third arm), indicated that all three MSPs are located within the very central region of M70. Imaging (see Figure 3) revealed a very bright, extended radio source near the center of the GC, which prevented us from confidently associating any of the MSPs with a compact radio source. However, a faint, compact source was also detected almost exactly at the cluster center. This source is a strong candidate for being associated with one of the MSPs. Dedicated timing follow-up is required to determine the precise positions of the MSPs and to confirm any association with the detected radio source.

The imaging of all GC fields observed in the GCGPS survey, including those that did not yield any MSP discoveries (see Figures 5, 6, and 7 in Appendix B), revealed several promising targets that could potentially host undiscovered MSPs. These candidates may have been missed in the original GCGPS search due to reduced sensitivity, particularly in the outer regions of the clusters. The processed FITS files corresponding to these images are published with this paper (doi:10.5281/zenodo.17781807) to support more focused, targeted follow-up efforts. Additionally, the imaging data were used to compute nondetection limits for each of the GCGPS-observed GCs using the radiometer equation (Equation (3)). Based on the respective observational parameters, the 10σ nondetection limits (both continuum and beamformed) for each cluster, at the observed uGMRT frequency band, are presented in Table 1.

Acknowledgments

We acknowledge the support of the Department of Atomic Energy, Government of India, under project No. 12-R&D-TFR5.02-0700. The GMRT is run by the National Centre for Radio Astrophysics of the Tata Institute of Fundamental Research, India. We thank the GMRT operators for their coordinated effort in conducting the GCGPS survey observations. P.C.C.F. gratefully acknowledges continuing support from the Max-Planck-Gesellschaft and hospitality of the Academia Sinica Institute of Astronomy and Astrophysics in Taipei, Taiwan, where part of this work was conducted while he was a Visiting Scholar. We also acknowledge support from the Building Indo-UK Collaborations toward the SKA program, which facilitated the development of the pulsar search pipeline, particularly the highly efficient GPU-based version. We acknowledge the contributions of the SPOTLIGHT team in the development of the pulsar search pipeline. SPOTLIGHT at the GMRT enables studies of pulsars and fast radio bursts (FRBs) using a petaflop-scale computing facility (called Param Brahmand) based on Param Rudra servers, funded by the National Supercomputing Mission of the Government of India. We especially thank our colleagues at C-DAC (Centre for Development of Advanced Computing) for their support in setting up the Param Brahmand data center at the GMRT.

Appendix A
PRESTO PREPFOLD Output of All Five Discovered MSPs

In this section (Figure 4) we provide all the highest-SNR folded profile plots from the discovery observation for all the GCGPS discovered five MSPs presented in this paper.

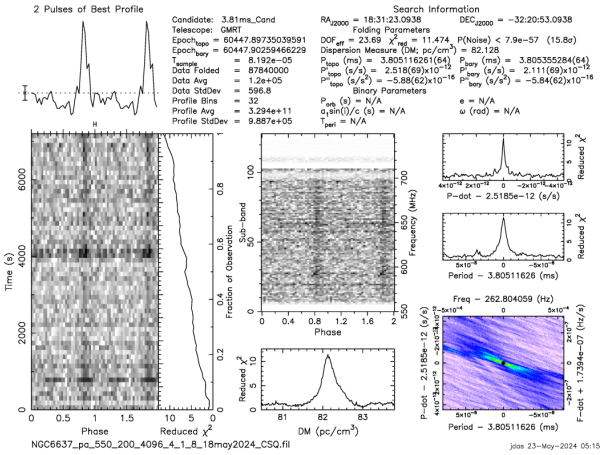

(a) J1831−3220A (M69A)

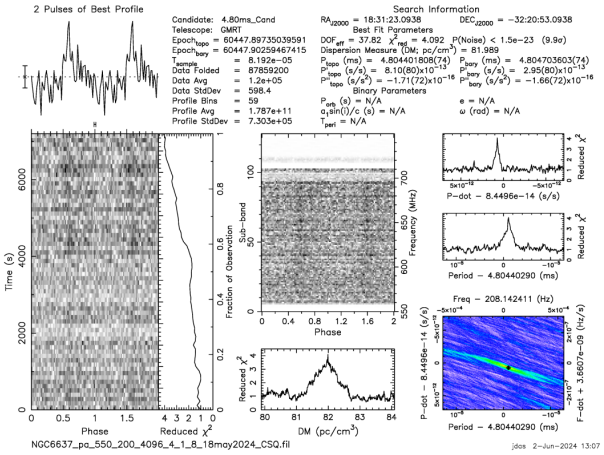

(b) J1831−3220B (M69B)

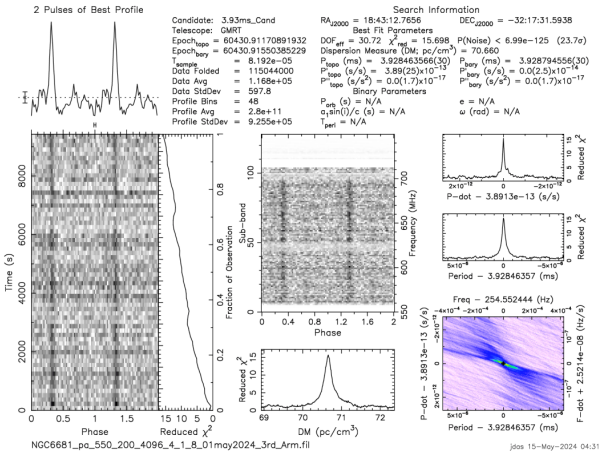

(c) J1843−3217A (M70A)

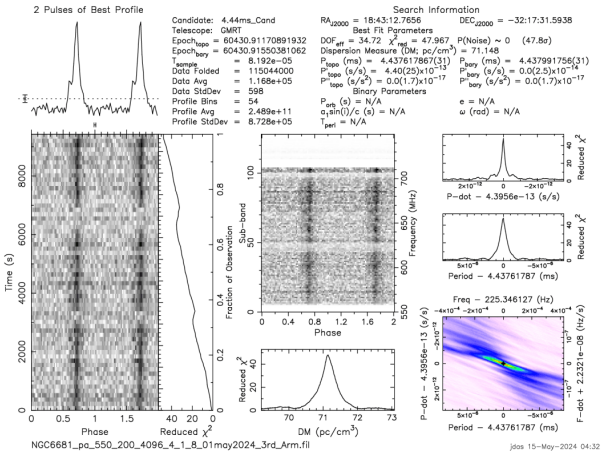

(d) J1843−3217B (M70B)

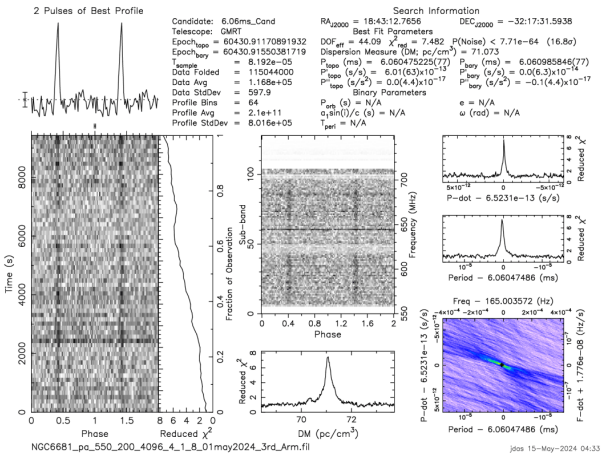

(e) J1843−3217C (M70C)

Figure 4. PRESTO PREPFOLD output for the highest-SNR beam from the discovery observations of the five newly discovered MSPs in M69 and M70.

Appendix B
Radio Continuum Images of GCGPS-observed GCs

In this section (Figures 5, 6, and 7), we present all the images of the GCs that we observed and analysed till now, which we use either to localize the discovered MSPs or to derive the non-detection limits (see Table 1) for the non-detections as well.

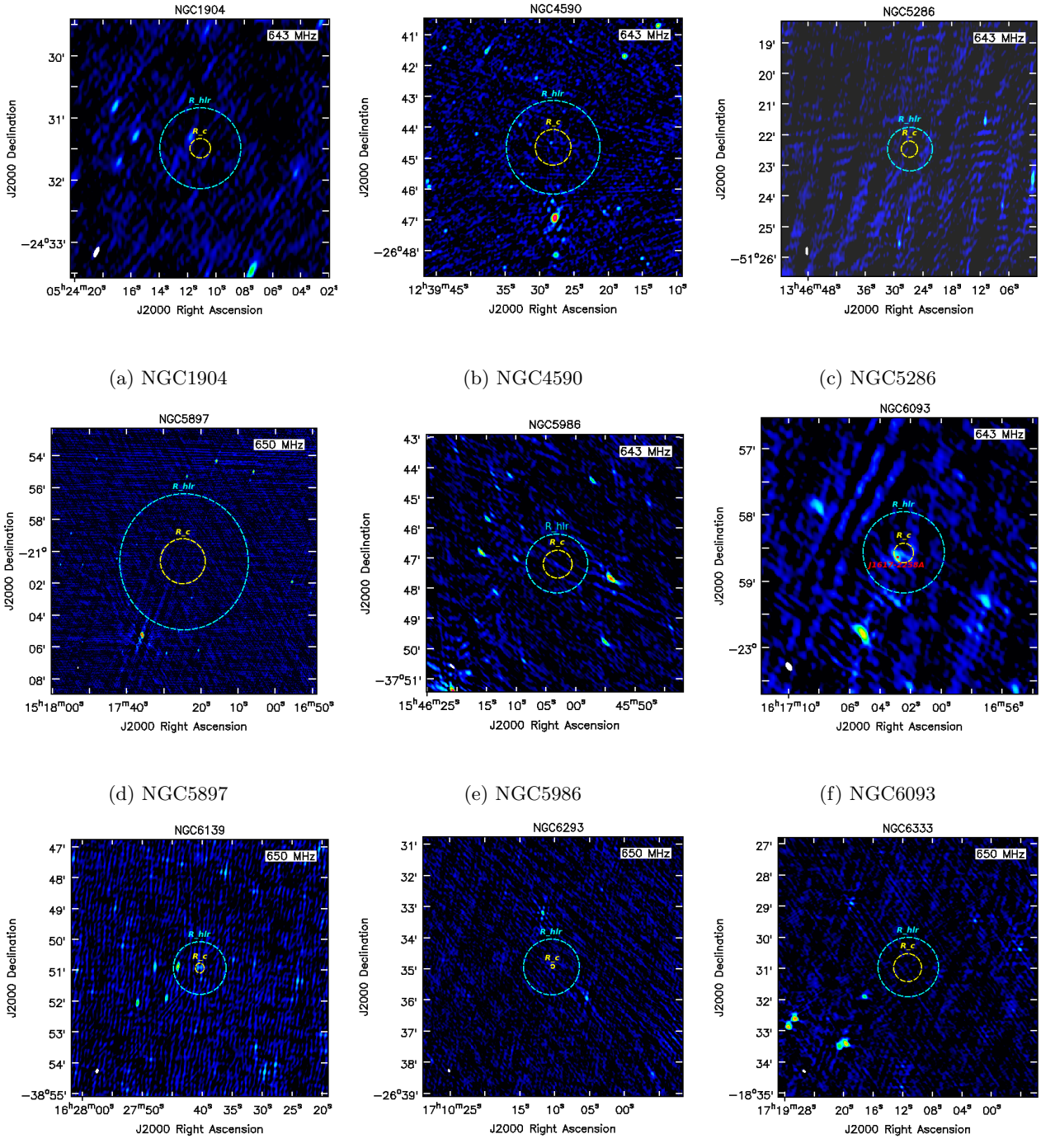

(a) NGC1904 (b) NGC4590 (c) NGC5286

(d) NGC5897 (e) NGC5986 (f) NGC6093

(g) NGC6139 (h) NGC6293 (i) NGC6333

Figure 5. Radio continuum images of the globular clusters observed in the GCGPS survey (Set 1). In each image (Set 1, as well as Sets 2 and 3 in the following figures), the dashed cyan circle denotes the half-light radius, $R_{\rm hlr}$, and the yellow circle marks the core radius, $R_{\rm c}$, indicating the core region of the cluster.

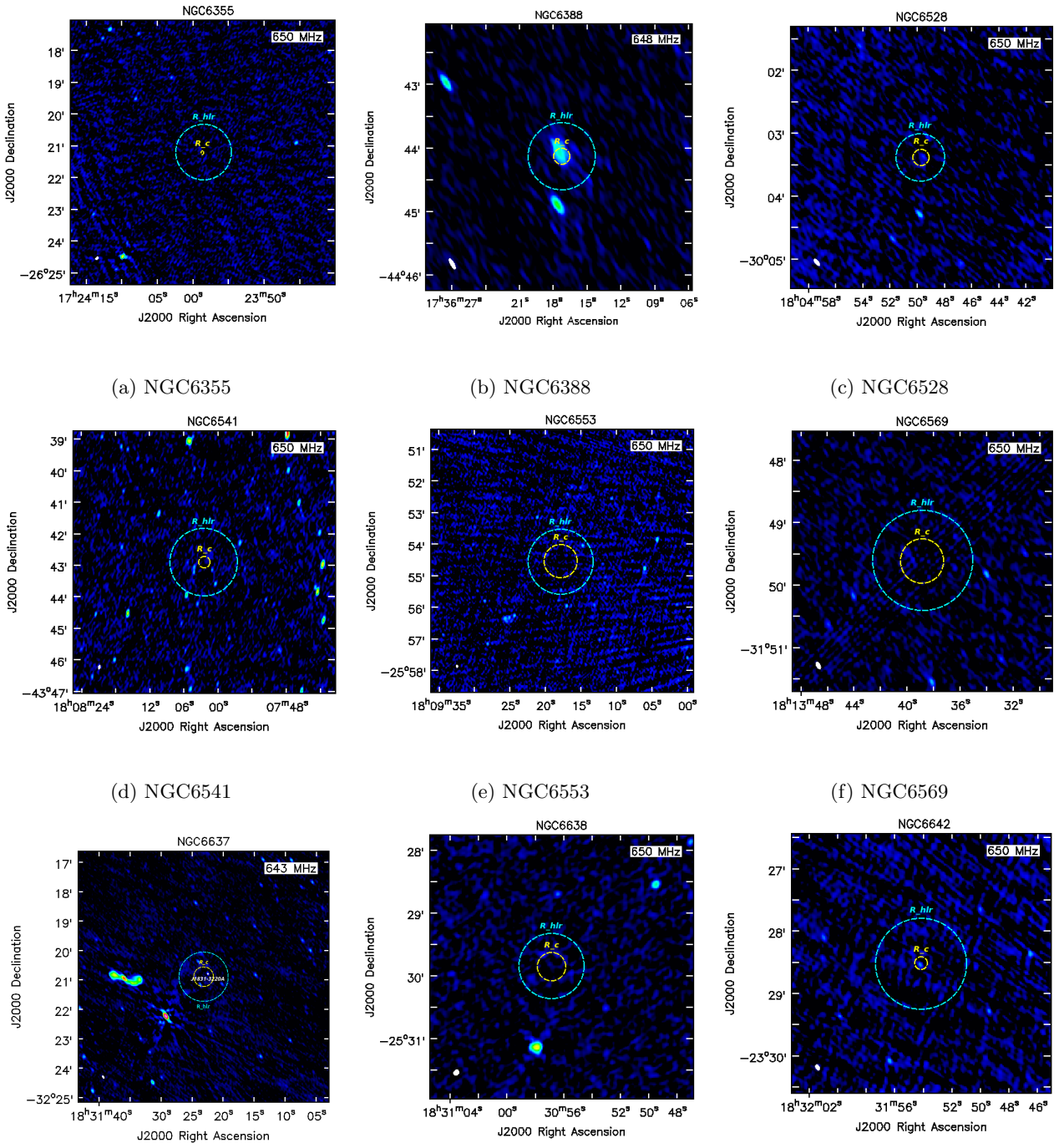

(a) NGC6355 (b) NGC6388 (c) NGC6528

(d) NGC6541 (e) NGC6553 (f) NGC6569

(g) NGC6637 (h) NGC6638 (i) NGC6642

Figure 6. Radio continuum images of GCs observed in the GCGPS survey (Set 2).

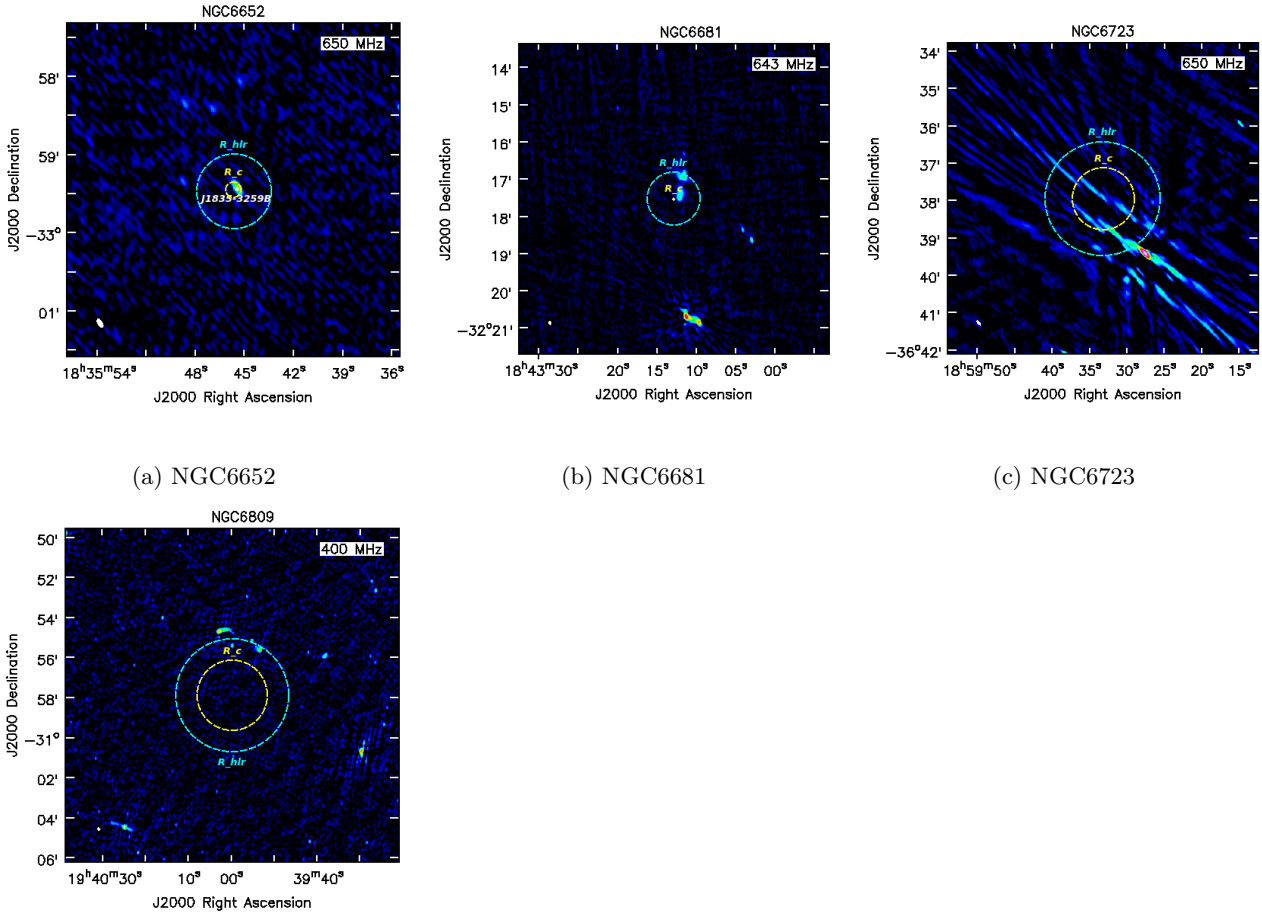

(a) NGC6652 (b) NGC6681 (c) NGC6723

(d) NGC6809

Figure 7. Radio continuum images of GCs observed in the GCGPS survey (Set 3).

ORCID iDs

Jyotirmoy Das https://orcid.org/0009-0006-7995-5871
Jayanta Roy https://orcid.org/0000-0002-2892-8025
Paulo C. C. Freire https://orcid.org/0000-0003-1307-9435
Scott Ransom https://orcid.org/0000-0001-5799-9714
Bhaswati Bhattacharyya https://orcid.org/0000-0002-6287-6900
Karel Adamek https://orcid.org/0000-0003-2797-0595
Wes Armour https://orcid.org/0000-0003-1756-3064
Sanjay Kudale https://orcid.org/0000-0002-6631-1077
Mekhala V. Muley https://orcid.org/0009-0008-1233-6915

References

Abbate, F., Ridolfi, A., Barr, E. D., et al. 2022, MNRAS, 513, 2292
Bahramian, A., Heinke, C. O., Sivakoff, G. R., & Gladstone, J. C. 2013, ApJ, 766, 136
Barr, E. D. 2018, IAUS, 337, 175
Barr, E. D., Dutta, A., Freire, P. C. C., et al. 2024, Sci, 383, 275
Becker, W., & Trümper, J. 1999, A&A, 341, 803
Chen, J., Cadelano, M., Pallanca, C., et al. 2023, ApJ, 948, 84
Chen, W., Barr, E., Karuppusamy, R., Kramer, M., & Stappers, B. 2021, JAI, 10, 2150013
Das, J., Roy, J., Freire, P. C. C., et al. 2025, ApJ, 988, 161
Dewey, R. J., Taylor, J. H., Weisberg, J. M., & Stokes, G. H. 1985, ApJL, 294, L25
Freire, P. C. C., & Wex, N. 2024, LRR, 27, 5
Gautam, T., Ridolfi, A., Freire, P. C. C., et al. 2022, A&A, 664, A54
Harris, W. E. 1996, AJ, 112, 1487
Istrate, A. G., Tauris, T. M., & Langer, N. 2014, A&A, 571, A45
Kalogera, V. 1998, ApJ, 493, 368
Kalogera, V., & Webbink, R. F. 1996, ApJ, 458, 301
Kalogera, V., & Webbink, R. F. 1998, ApJ, 493, 351
Manchester, R. N., Hobbs, G. B., Teoh, A., & Hobbs, M. 2005, AJ, 129, 1993
Pooley, D., Lewin, W. H. G., Anderson, S. F., et al. 2003, ApJL, 591, L131
Ransom, S. 2011, PRESTO: PulsaR Exploration and Search TOolkit, Astrophysics Source Code Library, ascl:1107.017
Ridolfi, A., Freire, P. C. C., Gautam, T., et al. 2022, A&A, 664, A27
Roy, J., Chengalur, J. N., Adamek, K., et al. 2024, in URSI Regional Conf. Radio Science (URSI-RCRS), 1
Sarazin, C. L., Kundu, A., Irwin, J. A., et al. 2003, ApJ, 595, 743
Tauris, T. M., & van den Heuvel, E. P. J. 2023, Physics of Binary Star Evolution: From Stars to X-ray Binaries and Gravitational Wave Sources (Princeton Univ. Press)
Verbunt, F., & Hut, P. 1987, IAUS, 125, 187
Yao, J. M., Manchester, R. N., & Wang, N. 2017, ApJ, 835, 29